N94-17357

LASER BEAM STEERING DEVICE

February 1993

M.E. Motamedi, A.P. Andrews, and W.J. Gunning

Rockwell International Science Center
1049 Camino Dos Rios
Thousand Oaks, CA 91360

ABSTRACT

Agile beam steering is a critical requirement for airborne and space based LIDAR and optical communication systems. Design and test results are presented for a compact beam steering device with low inertia which functions by dithering two complementary (positive and negative) binary optic microlens arrays relative to each other in directions orthogonal to the direction of light propagation. The miniaturized system has been demonstrated at scan frequencies as high as 300 Hz, generating a 13 x 13 spot array with a total field of view of 2.4°. The design is readily extendable to a 9.5° field of view and a 52 x 52 scan pattern. The system is compact—less than 2 in. on a side. Further size reductions are anticipated.

1.0 INTRODUCTION

High speed optical beam steering is a major challenge for space based LIDAR systems. If this function is performed mechanically using bulk optical components, the resulting systems are too heavy for the more demanding applications that require rapid optical beam steering. These applications require lower rotational and translational inertia and smaller component displacements. Binary optics beam steering systems fulfill these requirements, achieving a field of view of more than 10 degrees with only a fraction of a millimeter component translation.[1]

We report here test results of a miniature laser beam steering device designed to demonstrate the feasibility of the binary optic approach. The steering mechanism is based on dithering two complementary (positive and negative) binary optic microlens arrays. The first demonstration of this steering concept was reported by Lincoln Laboratory.[1] In this paper, we

[1] W. Goltsos and M. Holz, "Agile beam steering using binary optic microlens arrays", *Optical Engineering*, vol. 29, pp. 1392–1397, (1990).

PRECEDING PAGE BLANK NOT FILMED

present a miniaturized version using a pair of 6 mm-aperture, F/6, 8-level binary optic microlens arrays designed to operate at 0.632 μm wavelength. The current actuator design can scan the laser beam at rates of 200 Hz or greater. Beam steering is accomplished by translating the microlens arrays relative to each other in directions orthogonal to the direction of light propagation. The multiple coherent apertures result in a far field spot pattern of fixed points. The current system has demonstrated rapid scanning of a 13 x 13 spot array with a total field of view of 2.4°, and is readily extendable to a 9.5° field of view and a 52 x 52 spot pattern. The microlens arrays are individually driven in orthogonal directions by piezoelectric actuators. The current beam steering system is quite compact—less than 2 in. on a side—and careful redesign with custom designed actuators can lead to a further reduction in size.

We have evaluated the performance of this device and are now studying its suitability for various beam steering applications such as laser radar, laser communication, and optical scanning.

2.0 BEAM STEERING PRINCIPLE

Optical beam steering is based on the principle of the Galilean telescope. The configuration of the system is shown in Figure 1, where a positive lens is followed by a confocal negative lens. The focal length of the negative lens (F_n) is slightly smaller than the focal length of the positive lens (F_p) by an amount equal to the spacing between the two lenses. If the lenses are displaced laterally relative to each other, a plane wave incident along the optic axis will emerge collimated but tilted away from the optic axis. If the negative lens is displaced perpendicular to the optic axis by the amount of x_s, then the tilt angle θ is given by

$$\theta = \arctan \frac{x_s}{F_n} . \tag{1}$$

Let z_{sp} be the separation between the two lenses and F/# be the focal ratio F_p/d of the positive lens, where d is the diameter of the smaller lens. Then Eq. (1) can be rearranged to

$$\theta = \arctan \frac{x_s}{d(F/\#)-z_{sp}} . \tag{2}$$

In practice, ideally the spacing between the two lenses is decreased to minimize vignetting. To determine the maximum steering angle θ_{max}, z_{sp} in Eq. (2) can be neglected and both lenses can be assumed to have the same diameter and focal length (and consequently the same F/#). Therefore, Eq. (2) can be reduced to

$$\theta \approx \arctan \frac{x_s}{d(F/\#)} . \tag{3}$$

The optical system shown in Figure 1 has maximum efficiency at zero scan ($x_s = 0$). As the scan angle increases, the vignetting increases, and the maximum useful scan occurs at $x_s \approx d/2$, where θ_{max} from Eq. (3) becomes

$$\theta_{max} \approx \arctan \frac{1}{2(F/\#)} . \tag{4}$$

Equation (4) suggests that faster lenses (smaller F/#) increase the scan angle. For example, a pair of F/2 lenses (one inch in diameter) in the system shown in Figure 1 has a field of view (FOV) equal to ± 14°.

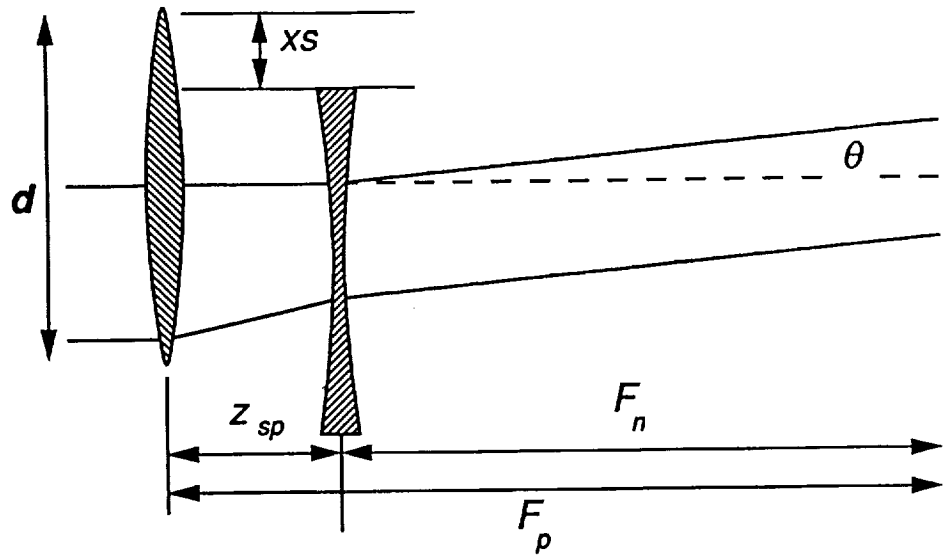

FIGURE 1. CONFIGURATION OF OPTICAL BEAM STEERING CONCEPT USING A PAIR OF GALILEAN CONFOCAL LENSES.

The system in Figure 1 has two drawbacks for optical beam steering: 1) the lenses are refractive, which limits the lens separation; and 2) the large lens diameter requires large translation (on the order of the lens diameter), which makes the system impractical for agile beam steering.

More agility is achieved by replacing the lenses of Figure 1 with a pair of complementary binary optic microlens arrays as shown in Figure 2. The microlens arrays are optically flat with surface relief on the order of one optical wavelength, permitting separation distances of several microns. Individual lenslet sizes can be in the range of 100–200 microns, resulting in maximum translation of similar magnitude. Reducing both the inertia and the travel of the lens system makes the device suitable for agile beam steering. Since Eq. (4) still holds for binary optics, the steering angle of the scanner can be very high. The multiple aperture design of the scanner results in a discrete spot scan pattern. The far field angular spot separation, $\Delta\theta$, is given by

$$\Delta\theta \sim \lambda/d \tag{5}$$

where d is the lenslet size, and the beam divergence, $\delta\theta$, is given by

$$\delta\theta \sim 2\lambda/D \tag{6}$$

where D is the beam diameter.

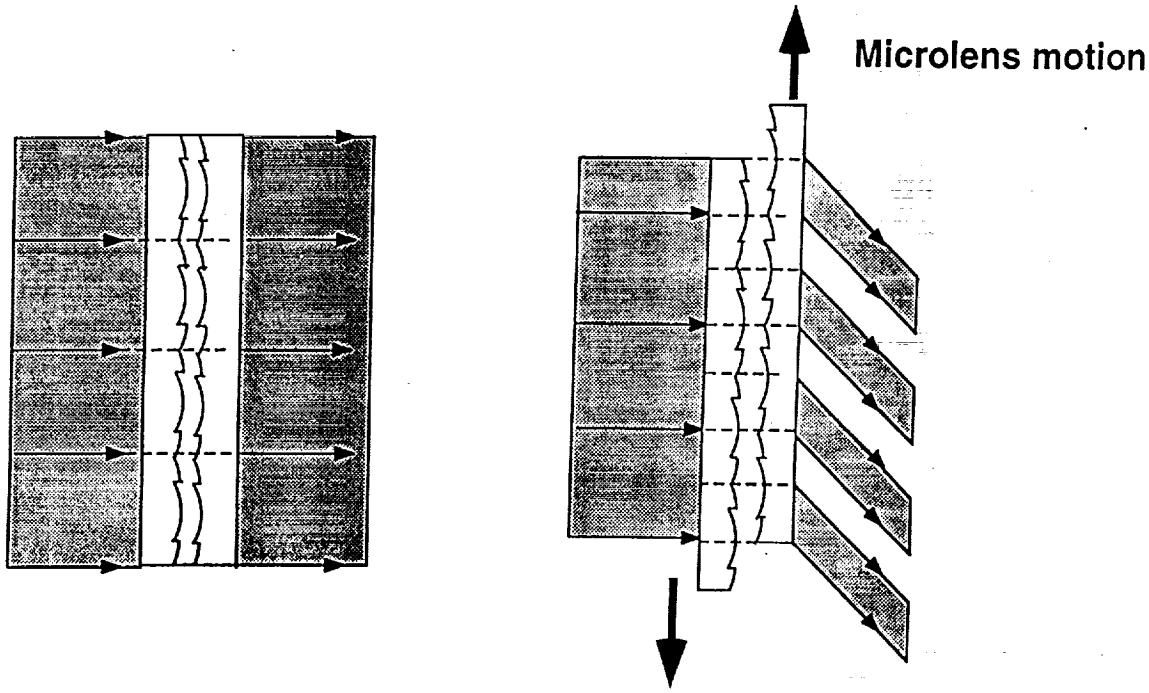

FIGURE 2. COMPLEMENTARY BINARY OPTIC MICROLENS ARRAYS FOR BEAM STEERING DEMONSTRATION.

3.0 BEAM STEERING THEORY

A binary optic[2] beam steering system based on the approach shown in Figure 2 has two parallel complementary microlens arrays spaced several microns apart. Input plane waves pass first through the positive microlens array and then through the negative microlens array. Since the spacing relative to the focal length is small, we can assume the two microlens arrays have the same focal length, f. From this assumption, both microlens arrays have the same F/# and the same microlens size.

Using the model of Sweatt,[3] the one-dimensional optical path function, g(x), can be written as

$$g(x) = \frac{cx^2}{1+\sqrt{1+(\hat{k}+1)c^2x^2}} \qquad (7)$$

[2]G. J. Swanson, "Binary Optics Technology: The Theory and Design of Multi-Level Diffraction Optical Elements", Tech. Report 854, Lincoln Laboratory, MIT, 14 August 1989.

[3]W.C. Sweatt, "Design holographic optical elements as lenses", *J. Opt. Soc. Am.*, Vol. 67 pp. 803-808, 1977.

where c is the surface curvature and $\hat{k}$ is a geometrical constant.

For a pure parabolic function, the value of $\hat{k} = -1$, and Eq. (7) reduces to

$$g(x) = \frac{cx^2}{2} . \tag{8}$$

For practical purposes when F/# is larger than F/4 in Eq. (8), the microlens phase function at the center wavelength, λ_o, can be reduced to

$$\phi_o = \frac{\pi x^2}{\lambda_o f} . \tag{9}$$

From Eq. (9), the microlens transmittance function at a wavelength λ can be shown to be

$$t(x) = \exp\left[\frac{j\pi}{\lambda f} x^2 \right] . \tag{10}$$

Equation (10) is the basic transmittance function for both binary optic microlenses. To formulate the field distribution of the binary optic beam steering system at the far field, we include an artificial imaging lens after the microlenses and evaluate the image at the focal plane. Figure 3 shows the schematic of this optical configuration.

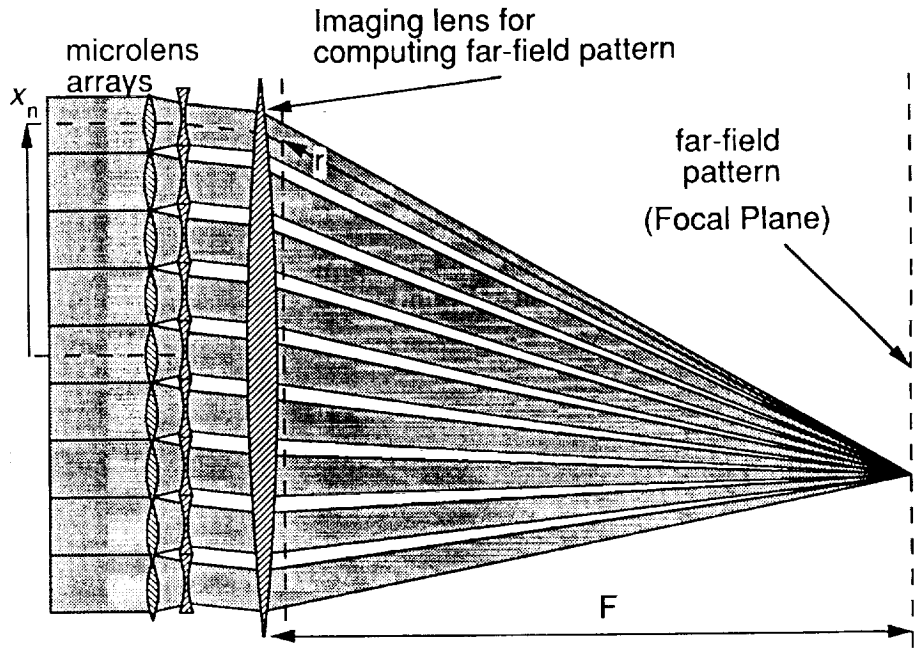

FIGURE 3. SCHEMATIC OF THE OPTICAL ARRANGEMENT FOR MICROOPTIC BEAM STEERING.

Applying Fourier optics[4] and considering the optical arrangement of Figure 3, the one-dimensional far-field pattern of the beam steering device can be shown to be

$$u(x)=u_o \sum_{-N}^{N} \int_{x_n-d/2}^{x_n+d/2} \exp\left[\frac{jk(x'-x_n)^2}{2f}\right]\exp\left[-\frac{jk(x'-(x_n+x_s))^2}{2f}\right]$$

$$\exp\left[\frac{jk\ x'^2}{2F}\right]\exp\left[-jk\sqrt{(x'-x)^2+F^2}\right]dx' \ . \qquad (11)$$

The first and second exponential factors in Eq. (11) represent the positive and negative microlens arrays, respectively. The variable x_s is the translation of the negative microlens relative to the positive microlens. The third exponential term represents the imaging lens, and the last exponential term is the propagation term. Note that f and F are the focal lengths of the binary optics microlens and imaging lens respectively, and the image plane is at the focal plane. N defines the size of the input beam and x' is the integration variable.

In evaluating u(x) at the far field, the focal length F is introduced for a mathematical model. Equation (11) can be reduced to the far-field intensity profile,

$$I(x) = u(x)\ u(x)^*$$

$$I(x)=I_o \sum_{-N}^{N} \exp\left[-\frac{jk\ x_n x_s}{f}\right] \int_{x_n-d/2}^{x_n+d/2} \exp[jk\ (x_s/f+x/F)x']dx' \ . \qquad (12)$$

For $x_r=x/F$, the formula (12) reduces to

$$I(x_r)=I_o \sum_{-N}^{N} \exp\left[-\frac{jk\ x_n x_s}{f}\right] \int_{x_n-d/2}^{x_n+d/2} \exp[jk\ (x_s/f+x_r)x']dx' \ . \qquad (13)$$

The angular scan due to x_r is generally on the order of a few milliradians. To view the behavior of Eq. (13), we plot $I(x_r)$ for $\pm$ 6 mrad, which covers at least two addressable points. Figure 4 shows the variation of $I(x_r)$ at the far field during a complete scan of one addressable point. Figure 4(a) is a plot of $I(x_r)$ at $x_s = 0$ (zero scan).

From Eq. (3), $x_s=(F/\#)\ \lambda$ at the first addressable point. For λ = 0.632 μm and F/# = F/6, the value of x_s is 3.79 μm. Figure 4(b) shows the $I(x_r)$ when the scanner has moved one addressable point; during the complete scan of 3.79 μm, the beam energy has been transferred to the next addressable point. During this transfer no portion of the total energy falls between the addressable points, as shown in Figure 4(b). Figure 4(c) is the superimposition of six plots of $I(x_r)$'s for x_s varying from 0 to 3.79 μm.

---

[4]J.W. Goodman, *Introduction to Fourier Optics*, McGraw Hill, New York (1968).

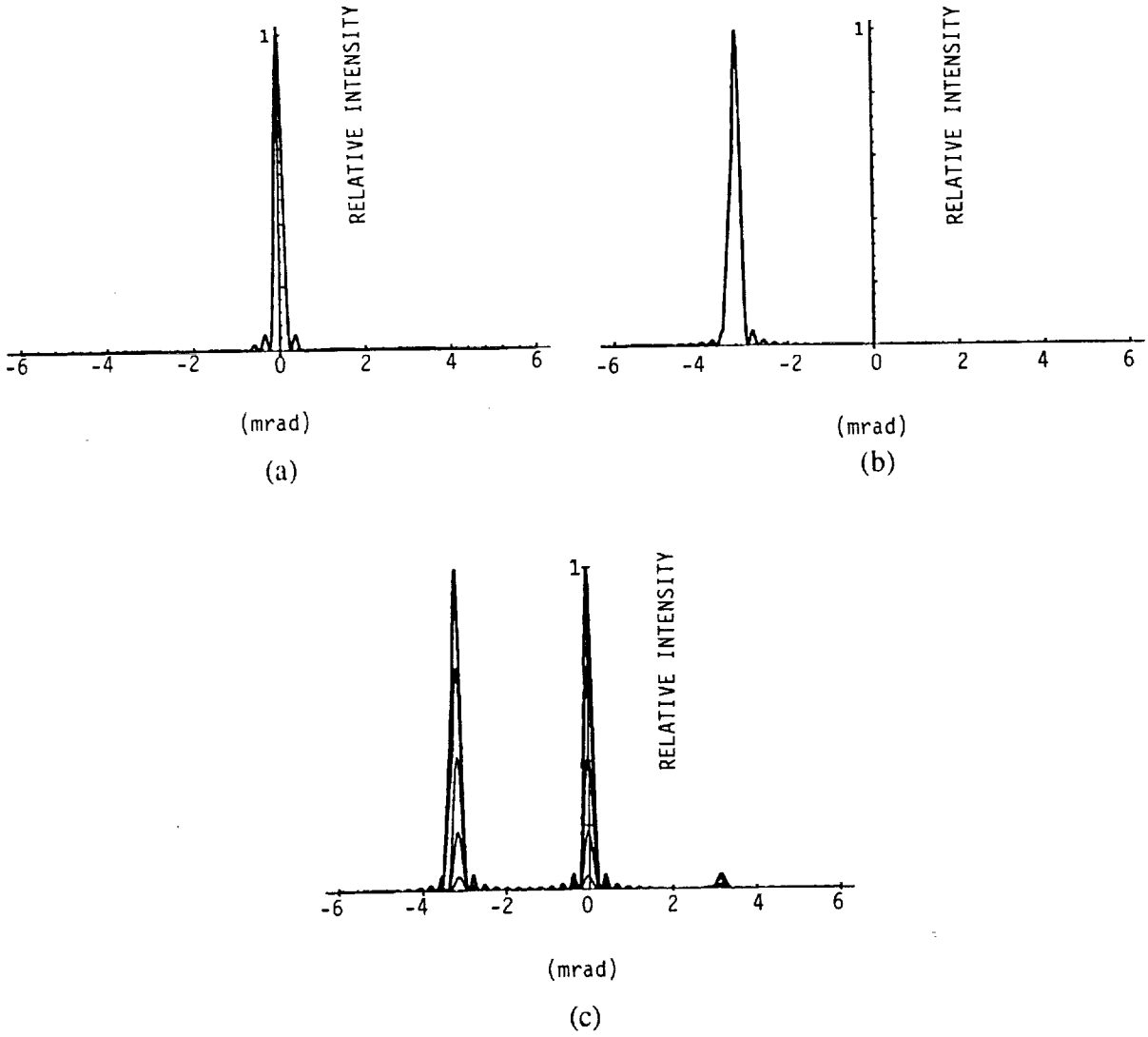

FIGURE 4. VARIATION OF $I(x_r)$ AT THE FAR FIELD DURING A COMPLETE SCAN OF ONE ADDRESSABLE POINT. (a) $I(x)$ AT $x_s=0$; (b) $I(x_r)$ AT $x_s= - 3.79\ \mu m$; (c) SIX SUPERIMPOSED PLOTS OF THE TRANSITION BETWEEN ADDRESSABLE POINTS.

Equation (13) is an integral solution to the behavior of the binary optic beam steering module shown in Figure 2. The relation (13) can be used to calculate the absolute intensity profile of the steering system at any far-field distance z where $z >> Nd$. This approach is more powerful than the approximation model used previously,[1] and it clearly demonstrates the effects of rotation errors, divergence and the near-field behavior of the binary optic beam steering system. More detailed theoretical results will be reported in a later paper.

4.0 BEAM STEERER DESIGN

The miniaturized beam steerer design uses simple parallelogram structures with orthogonal directions of translation for each microlens array. The basic design of this structure for one of the microlens arrays is illustrated in Figure 5. The structure is stiff in rotation and translation, except for rotations about the hinge lines. (The "hinges" of the parallelogram are actually flexible sections.) Each microlens array is mounted in a structure of this type, with their translation directions orthogonal to the optical axis and orthogonal to each other. By making the horizontal legs of the parallelogram sufficiently long, the variation in the spacing between the lenses over a complete scan could be held to tolerable levels during operation.

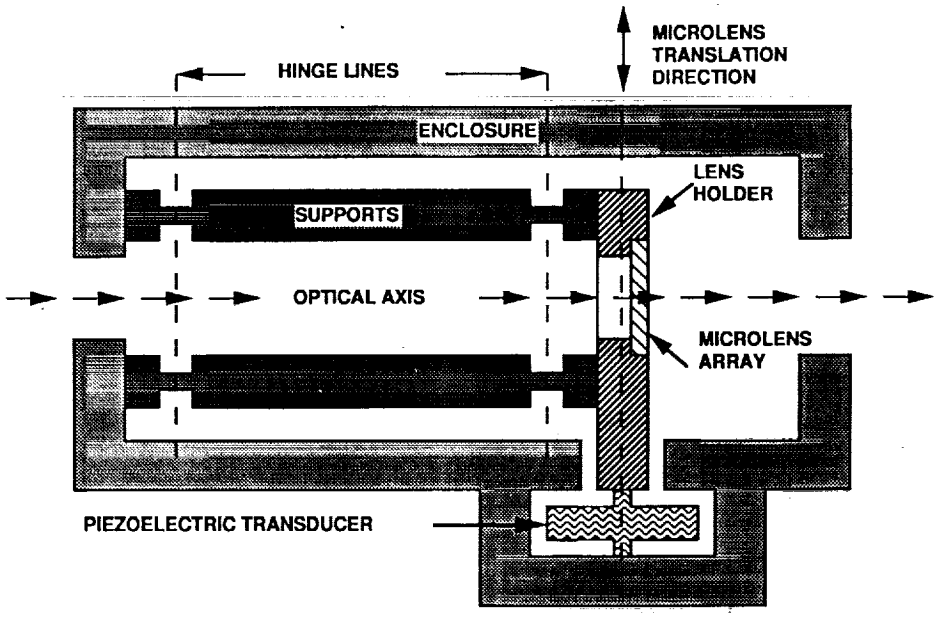

FIGURE 5. PARALLELOGRAM STRUCTURE FOR TRANSLATING MICROLENS ARRAYS.

Each microlens array is translated using a piezoelectric transducer mounted between the frame and the lens holder. Off-the-shelf transducers manufactured by Physik Instrumente (PI model P-288) were used for this demonstration. Smaller and faster devices can be designed using specialized transducers.

The microlenses were designed for a HeNe laser (λ = 0.632 μm). A low F/# is desirable. For an eight-phase-level binary optic microlens the minimum feature size is $2\lambda(F/\#)/8$.[5] For our 1 μm process, this places a lower limit of F/6 on the microlens F/#. The 32 x 32 arrays of 200 μm square microlenses have 100% fill factor. Flat quartz (better than $\lambda/8$) was used for the substrates. This design is predicted to produce a 52 x 52 spot scan pattern over a total square field of view of 9.5° x 9.5°. Spot separation and beam divergence are predicted to be, using Eqs. (5) and (6), 3.6 mrad and 506 μrad respectively.

[5]M.E. Motamedi, W.H. Southwell, R.J. Anderson, W.J. Gunning, M. Holz, " High Speed Binary Microlens in GaAs", *Proceedings* of SPIE, Vol. 1544, pp. 33–44, July 1991.

Binary Optic microlenses were designed as an approximation to a kinoform structure.[6] The binary lens profiles are generated by a stepwise multilevel etch process. As the number of phase levels is increased, the approximation of the kinoform structure is improved. A process consisting of m mask levels produces a structure having $M = 2^m$ phase levels. The etch depth of each mask level, d_i, is given by

$$d_i = \frac{\lambda}{(n-1)2^i} \tag{14}$$

where λ is the optical wavelength, n is the refracture index of the lens material, and i is the number of the individual mask level.

The theoretical diffraction efficiency of a kinoform lens is 100%, if reflection and obscuration losses are ignored. For a binary optic lens, the equivalent diffraction efficiency depends on the number of phase levels, M. This binary optic diffraction efficiency, η, is given by[2]

$$\eta = \left[\frac{\mathrm{Sin}\left(\frac{\pi}{M}\right)}{\left(\frac{\pi}{M}\right)} \right]^2 \tag{15}$$

where M is the total number of phase levels. Efficiency values for practical lenses are $\eta(M = 4) = 0.81$, $\eta(M = 8) = 0.95$, and $\eta(M = 16) = 0.99$.

The lenses operate over a small range in incident angle, so a simple planar holographic lens design was acceptable. The optical path difference (OPD) as a function of lens radius, r, is:

$$\mathrm{OPD}(r) = \sqrt{r^2 + f^2} - f, \tag{16}$$

where f is the focal length and the OPD is arbitrarily set to 0 for r = 0. Because this is a monotonic function in r, the quantization of the OPD for wavelength λ and parabolic phase function gives mask zones with radii

$$r(p, m) = \sqrt{2f\left(\frac{p\lambda}{2^m}\right)} \tag{17}$$

where p = 0,1,2,3... , and r(p, m) are the successive zone radii for the patterns in mask number m. These radii describe the edges of clear and opaque rings on the mask; for a positive lens, and with a positive photoresist as used here, the odd numbered zones give the outside of opaque rings. (The central zone of each mask, defined by p = 0 and p = 1, is an opaque disk.)[6]

The microlens profiles were designed to be parabolic to reduce aberrations. The focal lengths of the two lenses were adjusted to accommodate a nominal 5 μm separation, and the

[6]M.E. Motamedi, W.J. Gunning, M.P. Griswold, R.E. Knowlden, "Silicon Microlenses for Enhanced Optical Coupling to Silicon Focal Planes", *Proceedings* of SPIE, Vol. 1544, pp. 22–32, July 1991.

scanner was designed to maintain 5 ± 0.5 μm spacing between the microlens arrays. For this spacing, the focal length of the negative array is 1195 μm, and the positive array focal length is 1200 μm.

Each microlens was designed using 8 phase levels, which can be generated using three masks. An extra mask was used to fabricate three 10 x 10 x 3 μm platforms which are designed to prevent physical contact of the arrays and for adjusting array separation using interferometry.

5.0 EXPERIMENTAL RESULTS

The binary optic microlens arrays were fabricated out of fused quartz at MIT Lincoln Laboratory using photoresist masking and reactive ion etching (RIE). A mixture of CHF_3 and oxygen was used as the reactive working gas, producing a 200Å/min etch rate. Resist thickness was 5000Å. Thickness and alignment accuracy were measured after each photoresist development step. Etch depths for the three level process were 7020Å, 3510Å, and 1750Å respectively. The layer-to-layer misalignment was less than 0.2 μm and 0.3 μm for the positive and negative microlens arrays, respectively. The first measurement was determined by on-device micrometers located outside the boundaries of the arrays. The etch depth was controlled within 3%. Average step-to-step etch uniformity was better than 5%. Figure 6 shows a photomicrograph of the portion of the positive microlens array. The feature size at the corners of the lens is in the range of the 0.5 μm.

The microlens chips were sawed from the wafer in squares 10 mm on a side and 0.4 mm thick. The total mass of the microlens chip is 140 mg. Each microlens array is aligned to the sides of an opening into a lens holder. During this alignment procedure, the lens is held down by soft vacuum under elevated temperature to bring the bonding epoxy to the liquid phase. After the alignment cycle the temperature is reduced slowly to room temperature while the vacuum level increased. Figure 7 shows the assembled module. Figure 8 shows a close-up of the module aperture exposing the binary optic microlens arrays.

Each array is driven by a piezoelectric actuator, the two arrays being driven in orthogonal directions. The ultimate module field of view of 9.5° is achieved by translating the array by one-half of a lenslet diameter, which is ±100 μm. However, the compact actuators (PI model P-288) chosen for this demonstration have a maximum translation range of ± 25 μm. This allows the scanner to achieve a 13 x 13 spot pattern. A smaller laser scanner device (less than one cubic centimeter) can be designed using a custom actuator.

The beam steering module was tested using the optical setup shown in Figure 9. Light from a HeNe laser is passed through a collimator. Figure 10 shows a photograph of scanner output when both microlenses are aligned and they are parallel to each other with a negligible separation error. The center lobe contains most of the beam energy. The rest of the energy is distributed among the neighboring addressable points.

A desktop computer with a customized D/A converter board was used to generate drive signals for the scan actuators. Programmable patterns of test signals were output to the piezoelectric transducers to control the beam angle in two dimensions.

SCP-0152-A

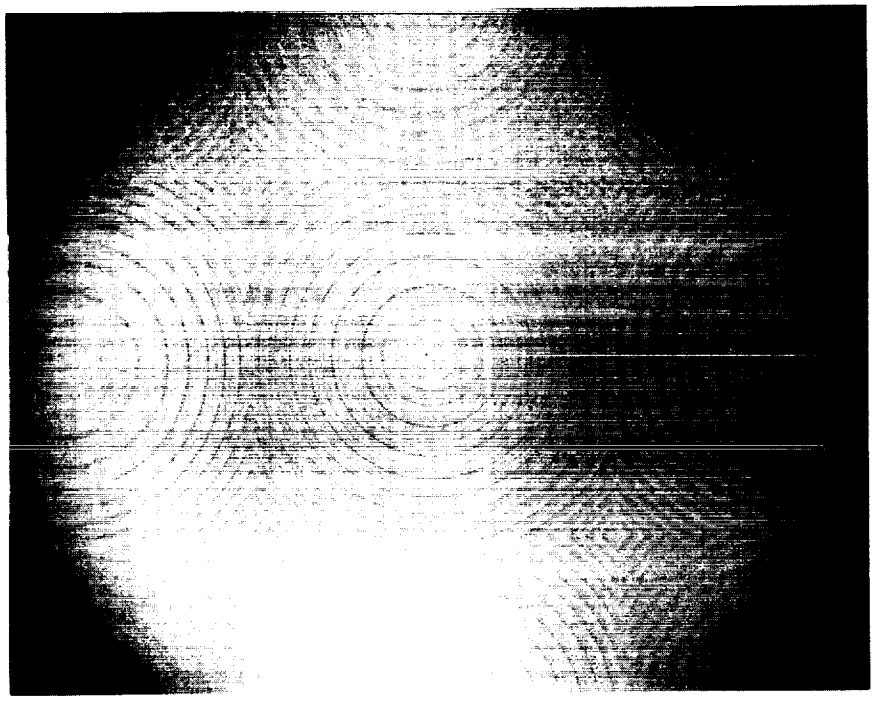

FIGURE 6. PHOTOMICROGRAPH OF MICROLENS ARRAY SEGMENT WITH 200 x 200 μm SQUARE MICROLENSES.

The result of a linear scan is shown in Figure 11. The resulting patterns showed, as predicted, very uniform and well-aligned spots where the majority of the energy is diffracted into a single peak with lesser amounts into neighboring peaks. In Figure 11, the first neighboring addressable points are also slightly illuminated. This is caused by higher diffraction orders, microlens separation error, and process nonuniformity.

The scanner was demonstrated up to a rate of 300 Hz. Operation at higher than 1 KHz is possible with appropriate damping of mechanical resonances.

The results of a spot scan of the energy distribution in the near field at 124 cm from the beam steerer, including a photograph at the same distance, are shown in Figure 11. The measurement showed that 50% of the transmitted energy appears in the principal diffraction lobe. A spot scan in the far field (7 m) resulted in measurements of angular spot separation of 3.6 mrad and beam divergence of 400 μrad, in good agreement with predicted values of 3.6 mrad and 506 μrad respectively.

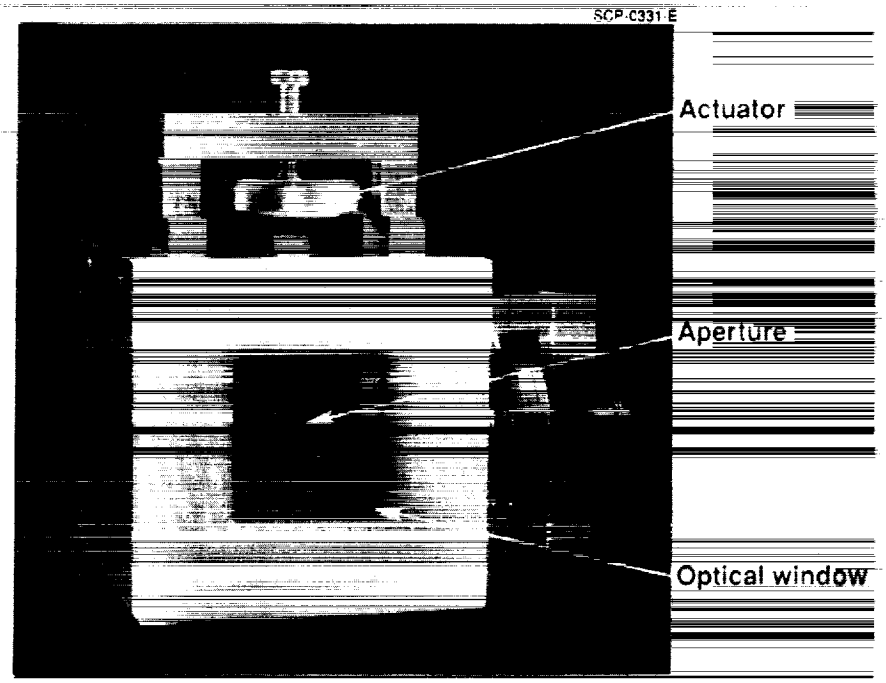

FIGURE 7. MINIATURIZED STEERING MODULE SHOWING PIEZOELECTRIC ACTUATORS.

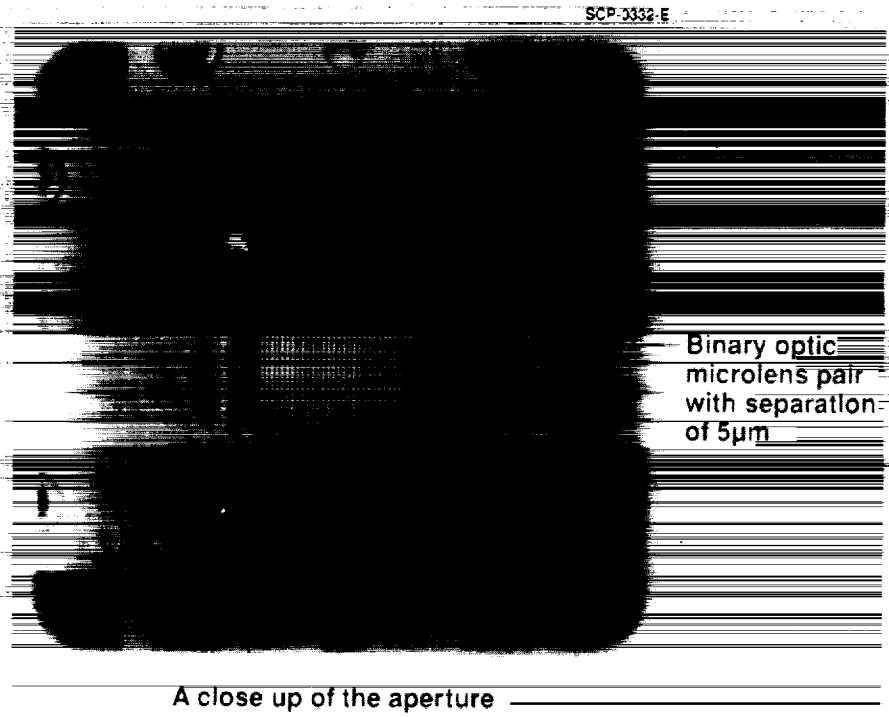

FIGURE 8. CLOSE-UP OF STEERING MODULE APERTURE, SHOWING MICROLENS ARRAYS.

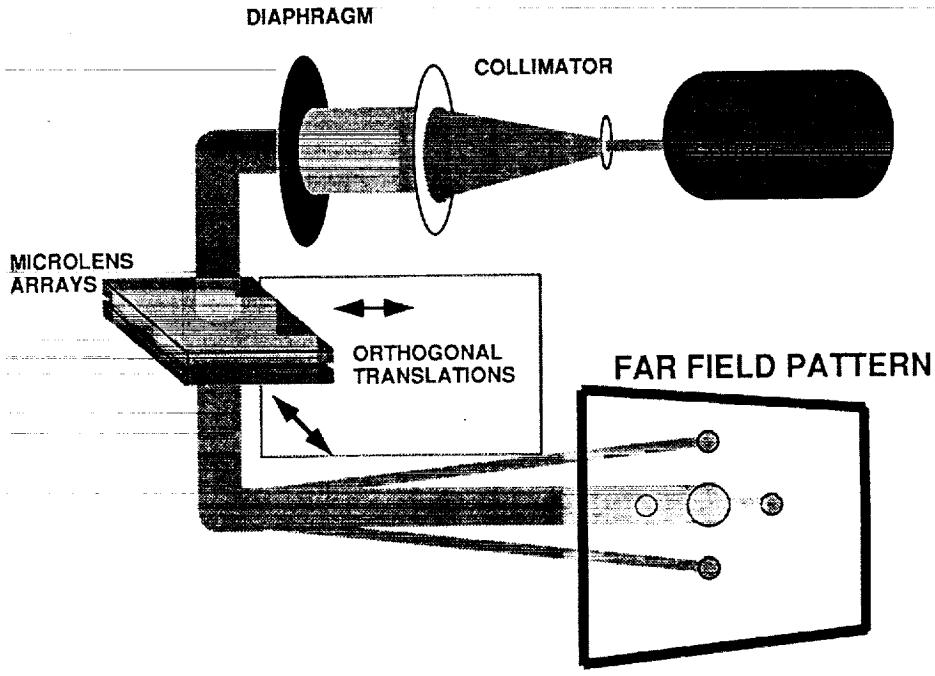

FIGURE 9. SCHEMATIC OF APPARATUS FOR MEASURING FIELD PATTERNS.

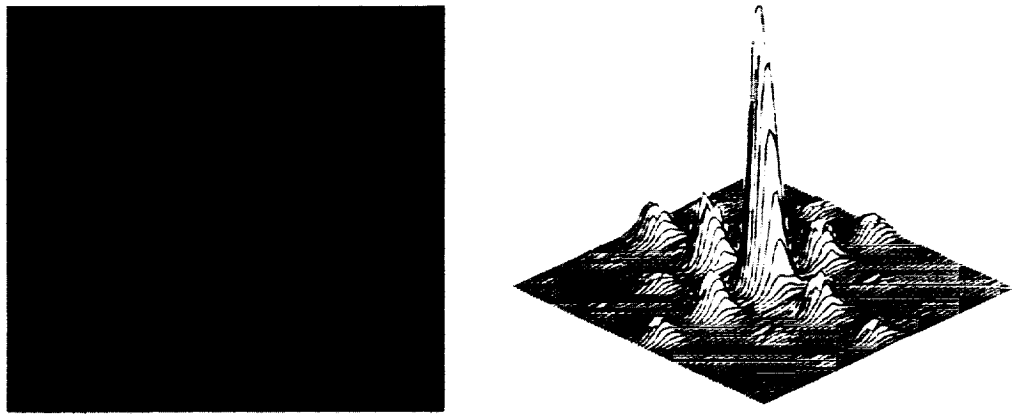

FIGURE 10. PHOTOGRAPH AND SPOT SCAN DATA OF FIELD PATTERN AT 124 cm FROM BEAM STEERER.

Linear Scan Demonstrated

Rockwell Beam Steering Module Characteristics

- **300 Hz scan rate demonstrated**
  - **Linear, X only, Y only**
  - **Diagonal X + Y**
  - **Random**
- **16 x 16 array demonstrated**

FIGURE 11. MULTICYCLE EXPOSURE OF LINEAR SCAN AT 200 Hz.

CONCLUSION

We have demonstrated that binary optics can be used to design a laser beam steerer that is small, lightweight, and agile. A demonstration device was fabricated and its optical and mechanical properties were verified. The resulting far-field pattern of the scanner showed a single intense spot that agreed well with the theoretical distribution. The scan rate is far superior to any demonstrated to date for this technology and illustrates its potential for laser beam steering applications.

ACKNOWLEDGMENT

The authors gratefully acknowledge the consistent support of Dr. Monte Khoshnevisan in making this research successful. Thanks are due Bill Southwell, Leonard Hale, and Eric Schonning at Rockwell Science Center; Pete Avizonis at Rockwell Strategic Defense Center; and Wilfred Veldkamp at Lincoln Laboratory. We also thank Margaret Stern and Bill Delaney at Lincoln Laboratory for their contribution to processing the microlenses; and Bob Knowlden, William Goltsos and Garret Nenninger from Lincoln Lab for their support in optical modeling and mask design. Thanks are also due to Rockwell Science Center co-workers Don Deakin for development of the microlens optical packaging and Bart Vanderlip for precision machining and assembly of the lens/actuator system.